CHEMISTRY OF MATERIALS

Article

pubs.acs.org/cm

Gold Nanooctahedra with Tunable Size and Microfluidic-Induced 3D Assembly for Highly Uniform SERS-Active Supercrystals

Sergio Gómez-Graña,[†] Cristina Fernández-López,[‡] Lakshminarayana Polavarapu,[‡] Jean-Baptiste Salmon,[†] Jacques Leng,[†] Isabel Pastoriza-Santos,*,[‡] and Jorge Pérez-Juste*,[‡]

[†]Université Bordeaux, Laboratoire du Futur, SOLVAY, CNRS, 178 avenue Schweitzer, F-33600 Pessac, France

[‡]Departamento de Química Física, Universidade de Vigo, Vigo 36310, Spain

Supporting Information

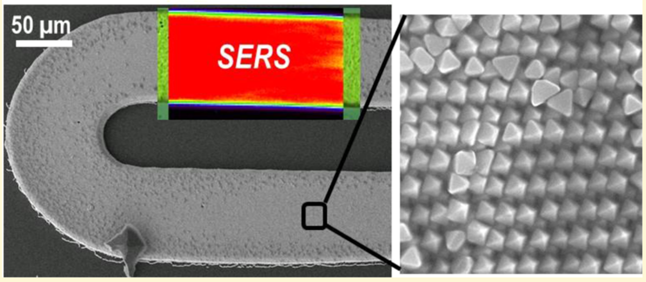

ABSTRACT: Shape-controlled synthesis of uniform noble metal nanoparticles (NPs) is crucial for the development of future plasmonic devices. The use of nanocrystals with well-defined morphologies and crystallinity as seed particles is expected to provide excellent shape control and monodispersity. We report the aqueous-based seed-mediated growth of monodisperse gold octahedra with wide range of sizes (50–150 nm in side length) by reducing different amounts of $HAuCl_4$ on preformed single crystalline gold nanorods using butenoic acid as reducing agent. Butenoic acid plays a key role as a mild reducing agent as well as favoring the thermodynamic control of the reaction. The uniformity of the as-prepared Au octahedra combined with the use of a microfluidic technique based on microevaporation will allow the self-assembly of octahedra into uniform 3D supercrystals. Additionally, these plasmonic substrates exhibit high and uniform SERS signals over extended areas with intensities increasing with the Au nanoparticle size.

INTRODUCTION

Over the years, colloidal plasmonic nanocrystals have emerged as important building blocks of modern nanoscience and nanotechnology to deal with a wide range of applications including electronics, energy, medicine, catalysis, biosensing, imaging, and therapy.[1−7] Most of these applications have been developed through the use of rich optical properties of plasmonic nanostructures that arise from the strong localized surface plasmon resonances (LSPRs).[1−6,8] The LSPR is strongly dependent on the shape of nanoparticles (NPs), among other parameters. Therefore, shape-controlled synthesis of noble metal nanocrystals has attracted great attention during the last two decades.[9,10] As a result numerous synthetic methods have been developed to prepare nanocrystals with different morphologies.[9,11,12] Among all, the seed-mediated growth approach has emerged as a reliable and versatile method for the preparation of a wide variety of morphologies such as spheres, rods, cubes, octahedra, decahedra, and triangles.[9,13,14] This technique is based on the overgrowth of preformed small nanoparticles (seed) via reduction a metal salt precursor with a mild reducing agent.[5,9,13] It has demonstrated that seed crystallinity is one of the main parameters determining the final NPs morphology.[9] Often, small particles (<2 nm) are used as seeds; however, it is extremely difficult to perfectly control the crystallinity of all the particles, which results in the formation of unwanted morphologies as byproduct. In addition, the seed-mediated growth mechanism of anisotropic NPs is unclear and still under intense investigation.[15,16] As a result, there has been a growing interest in using nanoparticles with well-defined morphologies as seeds to unveil the mechanistic paths of growth mechanism including the facet/site selective deposition of atoms during the overgrowth process.

In general, the overgrowth on NPs can be controlled either by fine-tuning the growth kinetics of the reaction or by directing the growth on specific facets using selective additives or capping molecules.[9,13,17,18] For instance, Xia and co-workers have reported the transformation of single-crystalline Ag nanospheres or nanocubes into octahedra by using citrate as capping molecule that binds strongly to the {111} facet, thereby facilitating the growth along the ⟨100⟩ direction.[18] Previously, our group has reported the overgrowth of single-crystalline Au nanorods (NRs) into octahedra[17] and pentatwinned Au NRs into truncated decahedra[19] using DMF as solvent, as well as, reducing agent in the presence of poly(vinylpyrrolidone) (PVP). The experimental conditions favored a thermodynamic control process. It is challenging to implement such shape transformations in aqueous medium. Very recently, Liu et al.[20] reported the overgrowth of Au NRs into Au octahedra by using ascorbic acid as reducing agent in the presence of Cu^{2+} ions at 60 °C. However, the high sensitivity of the reaction to the amount of Cu^{2+} ions does not allow the size range control. In order to realize the potential applications of plasmonic NPs, it is important to have a perfect shape control with excellent size tunability and reproducibility.

Received: September 15, 2015
Revised: October 8, 2015
Published: October 16, 2015

ACS Publications

DOI: 10.1021/acs.chemmater.5b03620
Chem. Mater. 2015, 27, 8310−8317

Scheme 1. Schematic Illustration of the Evaporation-Based Microfluidic Cell Used for Controlled Assembly of Au Octahedra[a]

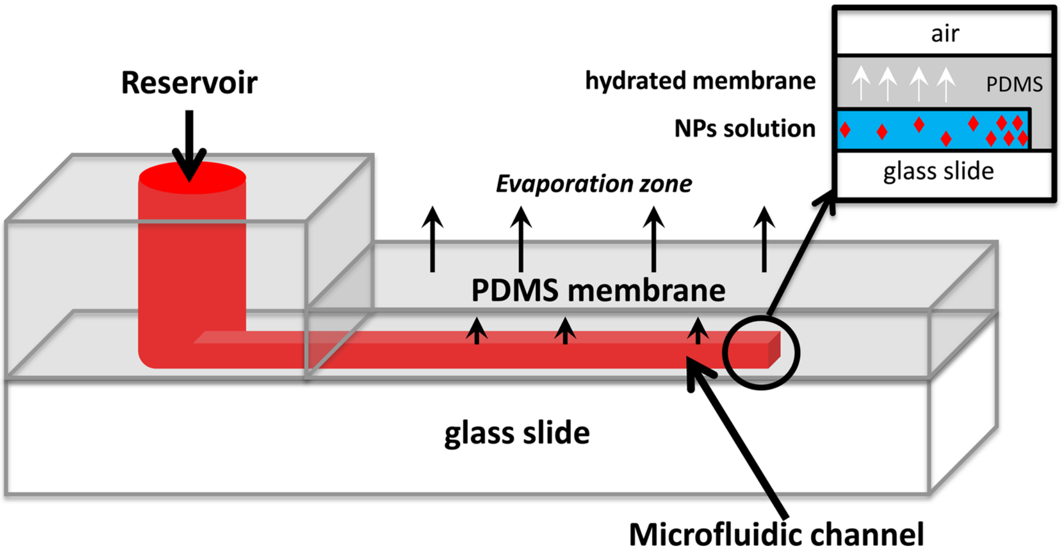

[a]Upon filling the microfluidic channel through the reservoir with a concentrated Au nanoparticle dispersion, the water evaporation proceeds across the thin PDMS membrane. It induces a concentration mechanism which gives rise to the nucleation and growth of a close-packed assembly of nanoparticles starting from the channel tip (see inset).

Surface-enhanced Raman scattering, SERS, is an advanced analytical technique that can be used for the ultrasensitive detection of various analytes related to biology, medicine, forensics, and environment.[21,22] SERS detection is based on the enhancement of Raman signals mainly by the strong electromagnetic fields at plasmonic surfaces. Although SERS has great potential for ultrasensitive detection, even up to the single molecular level, most of the applications are hampered by the inhomogeneity of the SERS signals. Recently, theoretical simulations have shown that when crystalline order is imposed on the assembly of nanoparticles, it may display antenna effects, leading to additional near-field enhancements and, therefore, higher SERS efficiencies.[23,24] The most common strategy to obtain 3D-supercrystal films on flat substrates is by drop-casting.[25] Nevertheless, it often leads to nonuniform films containing a wide distribution of domains with different thicknesses, sizes, and morphologies limiting their potential plasmonic applications.[26−28] Such a degree of crystalline order in which the NPs are close-packed can be achieved by using a microfluidic technique, such as microevaporation, to induce nanoparticle assembly.[29] Moreover, microfluidically induced assembly is a very promising approach to prepare uniform 3D assemblies of NPs of any dimensions using respective templates.[29]

We report here the aqueous synthesis of uniform Au octahedral NPs in high yield using presynthesized single-crystalline Au NRs as seeds and butenoic acid as a mild reducing agent in aqueous medium. Interestingly, butenoic acid could also act as capping agent through carboxylic groups adsorption, which leaves some vinyl groups available at NP surface for further surface modification, as it has been demonstrated by the grafting through polymerization of *N*-isopropylacrylamide.[30] This method additionally allows a wide tunability of the Au octahedra size (from 50 to 105 nm in side length) and, therefore, of their optical properties by simply varying the molar ratio of $HAuCl_4$ to Au NR seed (*R*). The size range could be easily extended at least until 150 in size length by using the preformed Au octahedra as seeds. Besides, we show that this approach can be easily extended to prepare Au decahedra by using pentatwinned Au NRs as seeds, indicating the general applicability of this approach as well as the importance of the seed crystallinity in the final NPs morphology. In addition to the Au octahedra synthesis, we further investigate their 3D assembly over extended areas into supercrystals using microfluidic-assisted assembly based on microevaporation, and their applicability as uniform SERS-active nanostructures. Additionally, the size effect of the Au octahedra building blocks in the SERS efficiency was evaluated.

■ EXPERIMENTAL SECTION

Materials. Silver nitrate ($AgNO_3$), gold(III) chloride trihydrate ($HAuCl_4.3H_2O$), hexadecyltrimethylammonium bromide (CTAB), benzyldimethylhexadecylammonium chloride (BDAC), L-ascorbic acid (AA), sodium borohydride ($NaBH_4$), hydrochloric acid (HCl), *N*-isopropylacrylamide (NIPAM), butenoic acid, and 1-naphthalenethiol (1-NAT) were purchased from Sigma-Aldrich. All chemicals were used as received.

Synthesis of Au Nanorods. Gold nanorods with a longitudinal surface plasmon resonance around 880 nm were prepared by the seed-mediated growth method.[31,32] In a typical synthesis, Au seed solution were prepared by quick addition of 0.3 mL (0.01 M) freshly prepared ice cold solution of $NaBH_4$ to an aqueous mixture of 4.7 mL (0.1 M) CTAB and 25 μL (0.05 M) $HAuCl_4$ solution under vigorous stirring. The stirring was continued for another 5 min, and the solution color turned to light brown. The resultant seed solution was kept at room temperature for 1 h before adding it into the growth solution. For the preparation of Au NRs, an aliquot of seed solution (24 μL) was added to a growth solution (10 mL) containing CTAB (0.1 M), $HAuCl_4$ (0.5 mM), ascorbic acid (0.8 mM), and silver nitrate (0.08 mM). The reaction flask was kept at 30 °C overnight in order to complete the Au NR growth process. The as-prepared Au NRs were purified by centrifugation (8500 rpm 25 min, twice) to remove the excess of reactants and surfactant remaining after the growth process. The purified Au NRs were

DOI: 10.1021/acs.chemmater.5b03620
Chem. Mater. 2015, 27, 8310−8317

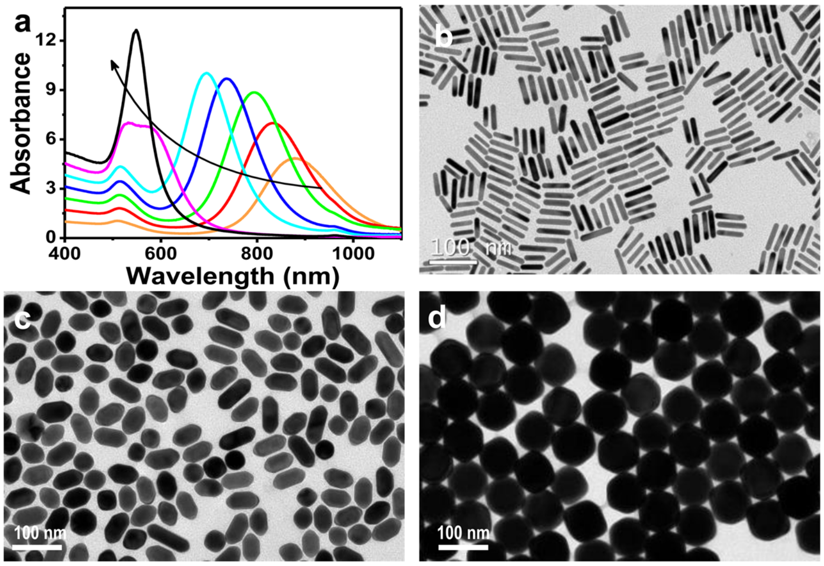

Figure 1. (a) Time evolution of visible−NIR spectra during the transformation of Au NRs (in orange) into octahedra (in black) in the presence of butenoic acid at 60 °C. The arrow shows the progress of the reaction. The total reaction time was 90 min. (b−d) TEM images showing the morphology of the Au nanoparticles in samples withdrawn at different reaction times: (b) 0, (c) 60, and (d) 90 min.

redispersed in 2 mL of 10 mM CTAB solution ([Au] = 2 mM, in terms of gold).

Synthesis of Au Octahedra. In a typical synthesis, 50 mL of 10 mM of CTAB (or BDAC) were mixed with 500 μL of 0.05 M $HAuCl_4$ and then 221 μL of butenoic acid (11.77 M) was added into the mixture to reduce the Au^{3+} to Au^{1+}. The reaction mixture was kept at 60 °C and the color of the solution gradually faded away (in about 3 or 35 min for CTAB or BDAC, respectively), indicating the Au^{3+} reduction (see Supporting Information Figure S1). Afterward, the purified Au nanorods were added as seeds and the reaction flask was kept at 60 °C overnight for the completion of Au octahedra growth. The final size of the gold octahedrons can be varied by changing the molar ratio (R) of gold salt to Au nanorods. The as prepared Au octahedra were washed by centrifugation (3000 rpm 30 min for R = 30), supernatant was discarded and the precipitate was redispersed in water. Table S1 in the Supporting Information summarizes the different ratios (R) investigated as well as the average side length of the octahedra and their surface plasmon resonances properties.

Microfluidic-Induced Assemblies of Au Octahedra. Microfluidic evaporation cells were created using standard soft photolithography technique.[33] A schematic representation for the preparation of microscopic-induced assemblies is shown in Scheme 1. At first, a master template was made with a photocurable resist and then polydimethylsiloxane (PDMS) thin membrane ($e \approx 100$ μm) was deposited on it by spin coating. The membrane was cured at 60 °C for 30 min. Additionally, a thick PDMS stamp was prepared in a Petri dish by pouring and curing PDMS at high temperature. The thick PDMS stamp was sealed on the thin PDMS membrane through plasma treatment and then peeled off from the template, and it was punched to create an opening for the reservoir. Finally, the PDMS chip was deposited on a clean microscope slide. Different microfluidic channels with 100 μm width, 7 μm height, and different lengths were tested and Au octahedra assemblies were prepared by injecting a concentrated aqueous dispersion of NPs ([Au] = 200 mM, in terms of gold) into microfluidic evaporators, followed by evaporation of the solvent only through the membrane. Finally, the PDMS template was peeled off of the glass slide in order to characterize the assemblies and study their SERS properties. In addition, the as-prepared assemblies on glass were treated under UV light (30 min) to remove organic surfactant present in the nanoparticles assemblies.

Characterization. The optical characterizations of Au NRs and octahedral NPs were carried out by with Agilent 8453 and Cary 5000 UV/vis/NIR spectrophotometer using 10 mm path length quartz cuvette. Transmission electron microscopy (TEM) images were obtained with a JEOL JEM 1010 transmission electron microscope operating at an acceleration voltage of 100 kV. Scanning electron microscopy (SEM) images have been obtained using a JEOL JSM-6700F FEG scanning electron microscope operating at an acceleration voltage of 15.0 kV in secondary-electron imaging (SEI) mode. The Electrospray ionization mass spectrometry (ESI-MS) was performed with a micrOTOF Focus (Bruker).

SERS characterization of the substrates were performed with 1-naphthalenethiol (1-NAT) as Raman probe and using a micro-Renishaw InVia Reflex system equipped with Peltier, a charge-coupled device (CCD) detector and three excitation different laser lines (633, 785, and 830 nm). At first, 1-NAT molecules were adsorbed on NP assemblies from the gas phase by casting a drop of 1-NAT in a Petri dish where the SERS substrates were also contained. The Petri dish was closed for 1 h in order to cover the 1-NAT molecules over the entire surface of the assemblies. SERS mappings were recorded on three different substrates made of three different sizes of Au octahedrons with 785 nm excitation and with a step size of 1 μm.

RESULTS AND DISCUSSION

Single-crystalline gold nanorods were synthesized using the well-established seed-mediated growth method based on the reduction of $HAuCl_4$ with ascorbic acid in the presence of cetyltrimethylammoniun bromide (CTAB), $AgNO_3$, and preformed tiny Au seeds (see Experimental Section for further details).[31] Figure 1b shows a TEM image of resulting Au

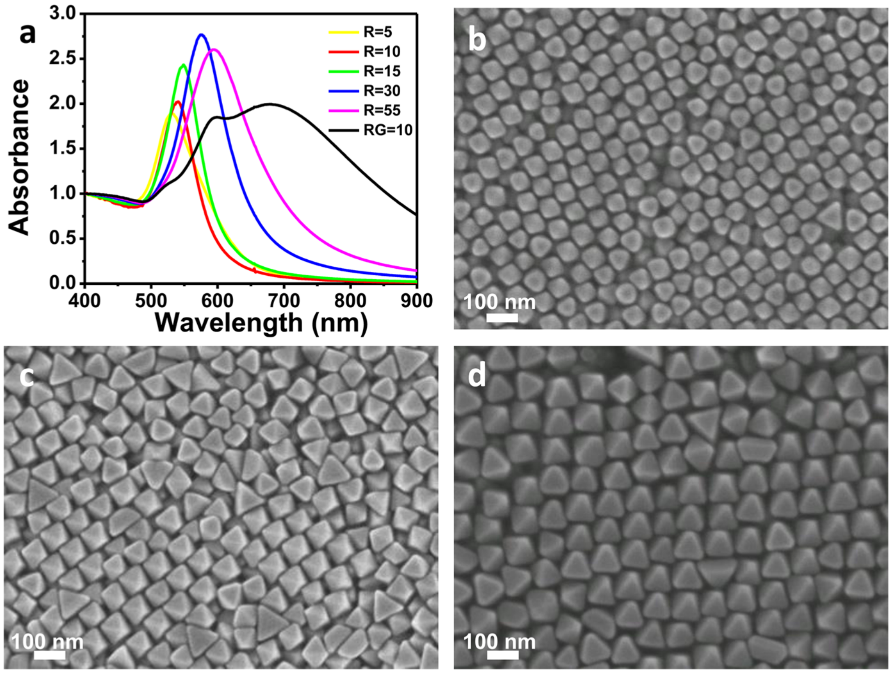

Figure 2. (a) Visible−NIR extinction spectra of Au octahedra prepared with different ratios between $HAuCl_4$/Au seed concentration, *R*, as indicated. The spectrum labeled as RG = 10 corresponds with a sample synthesized using the Au octahedra, obtained with *R* = 10, as seeds. (b−d) Representative SEM images of Au octahedra obtained with different $HAuCl_4$/seed ratios; (b) *R* = 15, (c) *R* = 30, and (d) *R* = 55.

nanorods with average dimensions of 68.4 ± 8.1 nm in length and 14.3 ± 1.6 nm in width. Then the Au NRs were overgrown to fabricate Au octahedra by reducing $HAuCl_4$ with butenoic acid in the presence of CTAB or benzyldimethylhexadecylammonium chloride (BDAC), as described in the Experimental Section. Thus, the addition of butenoic acid to an aqueous CTAB (or BDAC) solution of $HAuCl_4$ at 60 °C led to the gradual reduction of $AuCl_4^-$ to $AuCl_2^-$ as indicated by the damping of the $AuCl_4$−CTA (or $AuCl_4$−BDA) charge transfer to solvent (CTTS) absorption band at 400 nm (see Supporting Information Figure S1). Although similar results were obtained with BDAC and CTAB, the reduction of $AuCl_4^-$ to $AuCl_2^-$ took place faster in the case of using CTAB (1 min versus 27 min, Supporting Information Figure S1). Once all the $AuCl_4^-$ was reduced to $AuCl_2^-$, Au NRs were added initiating the catalytic reduction of Au(I) on their surface. It should be pointed out that the addition of Au nanorods prior to complete reduction to $AuCl_2^-$ resulted in oxidation of the seeds to $AuCl_2^-$ mediated by the $AuCl_4$−CTA (or $AuCl_4$−BDA) complexes.[34] The catalytic reduction of $AuCl_2^-$ led to gradual changes in the morphology of the nanorods as indicated the analysis of their optical properties by vis−NIR spectroscopy (Figure 1a). The extinction spectrum of initial Au NRs presented two distinct peaks at 525 and 880 nm, which were attributed to transversal and longitudinal LSPR, respectively. As the reaction proceeded, the longitudinal LSPR band of Au NRs gradually underwent a blue shift until it finally merged with the transversal LSPR into a single band. Transmission electron microscopy (TEM) analysis of aliquots collected at different reaction times confirmed that the observed spectral changes were due to the gradual transition of Au NRs into octahedra (Figure 1b−d). Therefore, the gradual blue shift of the longitudinal LSPR band was caused by the steady decrease of Au NRs aspect ratio,[17,20] and sharpening at the apexes and the merging of both longitudinal and transverse peaks into a single LSPR peak corresponded to the complete transformation into octahedra (see Figure 1b−d).

Moreover this protocol allowed to prepare highly uniform Au octahedra with a range of sizes by simply varying the molar ratio of $HAuCl_4$ to Au seed (*R*). Figure 2a shows the typical visible−NIR spectra of Au octahedra obtained with different *R* values (*R* = 5, 10, 15, 30, and 55), where a red shift and broadening in the LSPR band with the increase of R value is clearly observed. For instance, Au particles obtained at low *R* values (*R* = 5) presented the LSPR maximum centered at 530 nm, while those obtained at high *R* values (*R* = 55) at 597 nm. It indicated an increase in the side length of Au octahedra with *R*, as was confirmed by electron microscopies (see scanning electron microscopy, SEM, images in Figure 2 and TEM images in Supporting Information Figure S2 and Table S1). Besides, the measurement from TEM of the particle size and its standard deviation for different *R* values clearly indicated that this strategy allows to obtain Au octahedra with uniform size and tight size control in a size range from 50 to 105 nm. The uniformity of the samples is also reflected in the formation of close-packed well-ordered assemblies observed in the SEM images shown in Figure 2. In addition, the size range of Au octahedra could be further increased without affecting their quality by using preformed octahedra NPs as seeds. For example, Au octahedra with side length of ca. 136 nm were prepared with *R* = 10 but using preformed octahedrons of 60 nm in side length (synthesized with *R* = 10) as seeds. In this case, the overgrowth of the Au octahedral seeds not only cause the LSPR red shift and band broadening but also the appearance of a new band corresponding to a quadrupolar resonance (see red (seeds) and black (final particles) spectra, in Figure 2a).

Pentatwinned gold nanorods were also used as seeds instead of single-crystalline Au NRs, whereas the other reaction parameters remained the same. Pentatwinned gold nanorods

Scheme 2. Illustration Showing the Gradual Transformation of Au NRs into Octahedra via the Catalytic Reduction of the Gold Salt on the Au NR Surface[a]

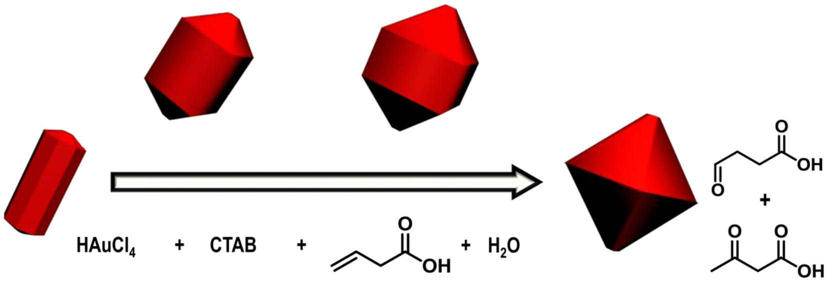

[a]It is accompanied by the oxidation of butenoic acid, reducing agent, to succinic semialdehyde or acetoacetic acid.

are enclosed by five {100} lateral facets, and the tips are enclosed by five {111} facets.[19] As for the single-crystalline gold nanorods, the butenoic-acid-mediated overgrowth produced a gradual blue shift of the longitudinal LSPR that eventually merged with the transversal LSPR becoming one single peak (Supporting Information Figure S3). TEM and SEM micrographs at different growth steps clearly showed the gradual decrease of Au NRs aspect ratio until the complete transition of Au NR to decahedrons (Supporting Information Figure S3).

To understand the mechanism and the role of butenoic acid in the transition of Au NRs-to-octahedra through the reduction of Au^{3+} in an aqueous surfactant solution, mass spectra of butenoic acid and the corresponding product were measured and analyzed. In these studies, the molar ratio of HAuCl$_4$ to butenoic acid was 1:1 instead of 1:104 (used in the Au NPs preparation; see Experimental Section for details). This modification would allow us to easily identify the final products of the reduction. It should be pointed out that previously, Xia and co-workers reported that Au^{3+} could be reduced to Au^{0} in aqueous medium by molecules containing vinyl groups, such as *N*-vinylpyrrolidone and *N*-isopropylacrylamide, leading to the formation of carboxylic acid as side groups.[35] In our case, the electrospray ionization mass spectrum of pure butenoic acid showed a molecular ion peak at m/z 87 attributed to its positive-ion mode (see Supporting Information Figure S4a), whereas that of the final product, the oxidized form of the butenoic acid, showed the peak at m/z 103 (Supporting Information Figure S4b). Nevertheless, these results revealed that the oxidized form had to be different from that proposed by Xia and co-workers,[35] 1,4-dibutanoic acid with 118.09 molecular weight. It has been also reported that in the presence of noble metal ions such PdCl$_2$ or AuCl$_4^-$, terminal alkenes could be catalytically transform into an aldehyde or ketone (Tsuji−Wacker oxidation reaction).[36] This pathway in the case of the butenoic acid oxidation would lead to the formation of either succinic semialdehyde or acetoacetic acid (see Scheme 2), both with a molecular weight of 102. Because the electrospray ionization mass spectrum of the product presented a molecular ion peak at m/z 103, we ascribed it to the positive-ion mode of either the aldehyde or the ketone product (Supporting Information Figure S4b). Scheme 2 shows an illustration of the overall process where the gold rod-to-octahedron transformation is accompanied by the Tsuji−Wacker oxidation of butenoic acid.

In order to understand the additional key role of butenoic acid in the formation and stabilization of {111} facets, control experiments were performed with other reducing agents, ascorbic acid, and *N*-isopropylacrylamide (NIPAM, a vinyl-containing molecule). In both cases, the other reaction parameters such as surfactant concentration, temperature, and *R* were kept constant. Although the use of *N*-isopropylacrylamide (NIPAM) as reducing agent led to gold nanospheres (Supporting Information Figure S5), with the ascorbic acid the resulting particles retained the nanorod shape but with a shorter aspect ratio indicating the homogeneous Au atom deposition along all Au NRs facets (Supporting Information Figure S5). These results clearly suggested that butenoic acid is a parameter that not only promoted the catalytic reduction of the gold salt on gold nanorods but also favored a thermodynamic controlled overgrowth. As shown in Scheme 2, the high-order {250} lateral facets, less stable than {111} and {110} tip facets, grow faster, yielding NRs with four {110} lateral facets and four {111} facets in each tip. The further growth of the {110} lateral facets gives the final octahedral structure bound by {111} facets.[17,37]

The high uniformity and tight control of the Au nanoparticle size make them excellent candidates to fabricate supercrystals. The assembly of Au octahedra into 3D structures was performed using a microfluidic technique based on evaporation, microevaporation, previously developed by Leng et al.[29,38] but with some modifications (see Scheme 1 and Experimental Section for more details). An end-closed microchannel connected to a reservoir was fabricated using a soft photolithography technique (Scheme 1). Then, 40 μL of a concentrated aqueous dispersion of 0.2 M Au NPs (in terms of gold) were injected through the reservoir into a microfluidic channel with 7 μm height and 100 μm width (Scheme 1). The evaporation of the solvent occurring across the PDMS membrane created a compensation flux coming from the reservoir driving the Au octahedra toward the tip of the microfluidic channel. Eventually, upon sufficient octahedra accumulation at the microchannel tip, a dense state of nanoparticles nucleated and grew into 3D assemblies of NPs (Scheme 1).[29] After the drying process, the PDMS template was carefully removed and the nanoparticle assembly was retained on the glass slide. SEM analysis (Figure 3) revealed that this microfluidic technique allowed obtaining densely close-packed supercrystals with morphologies that replicated the PDMS template over several millimeters long. SEM images from Figure 3 corresponds to a 3D assembly fabricated using Au octahedra with ca. 83 nm in side length (R = 30). The assembly showed a close-packed Au nanoparticle array. The fast Fourier transform of the SEM images confirm a perfect hexagonal geometry, allowing us to determine the average distance between the centers of neighboring metal particles (see Figure S6). In comparison with the assemblies obtained by

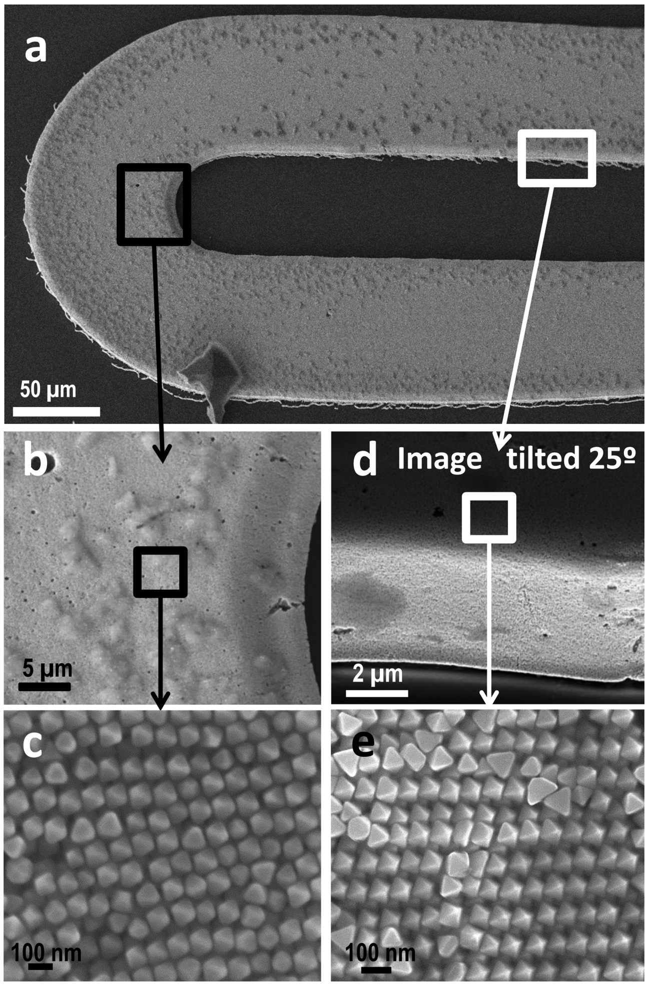

Figure 3. SEM images of self-assembled Au octahedra (ca. 83 nm in side length) fabricated by microevaporation after PDMS removal. (a) Top view of the microfluidic channel at low magnification (915 μm length, 100 μm width, and 7 μm height). (b−c) SEM micrographs collected from the selected areas highlighted by the black boxes. (d−e) SEM micrographs collected from the selected areas highlighted by the white boxes. The image in (d) was collected at a 25° tilt angle.

drop-casting technique with and without template, a remarkable improvement in the homogeneity, density, and large-areas can be clearly acquired through the present approach.[39] For instance, the assembly shown in Figure 3a has a length close to 1 mm, an average width of 100 μm, and an average height of 7 μm. In addition, this process can be easily extended to prepare assemblies of arbitrary dimensions and geometries denoted by the master template. A similar procedure, applied to Au octahedral particles with different sizes, obtained similar results.

Supercrystal structures made of plasmonic nanoparticles are particularly interesting in SERS due to the formation of dense hot spots as well as electric field migration within supercrystals.[3,27] Often, the main limitation of these plasmonic supercrystals is the lack of uniformity, which causes reproducibility problems.[26,27] As discussed above, the present approach allowed us to prepare large area assemblies of arbitrary macroscopic dimensions just by changing the microfluidic chip, which motivated us to investigate the SERS efficiency and uniformity on such substrates, a key requirement for the realization of quantitative SERS.[40,41] Thus, supercrystals fabricated using Au octahedra with average side lengths of 69 ± 5 nm, 83 ± 8 nm, and 136 ± 6 nm were selected to perform the SERS analysis. The Raman active probe, 1-naphthalenethiol (1-NAT), was deposited from the gas phase (see Experimental Section) in order to control the thiol molecules density on the Au octahedra-based substrates as well as to avoid any kind of substrate damage, which could result in a misleading interpretation of the SERS activity. Figure 4a shows the normalized SERS spectra of 1-NAT obtained exciting at 785 nm the substrates prepared with the Au octahedra of ca. 69, 84, and 136 nm. The spectra show the typical fingerprint vibrational peaks of 1-NAT, including the peaks for ring stretching (1372, 1501, and 1552 cm^{-1}), ring breathing (818 and 964 cm^{-1}), ring deformation (514, 536, and 660 cm^{-1}), C−S stretching (396 cm^{-1}), and C−H bending (1194 cm^{-1}). As depicted in Figure 4a, the SERS efficiency of the assemblies increased with the size of Au octahedra, indicating that the field enhancement at the excitation wavelength (785 nm) increased with Au nanoparticle size. Although it has been proposed that nanoparticles with smaller size would mean larger amount of smaller gaps (or hot spots) between the particles, we also need to bear in mind that a gap between larger particles will produce higher enhancements than the same gap between smaller particles. Thus, two opposite contributions have to be considered to understand such enhancements; on the one hand, the number of hot spots, and on the other hand, the enhancement factor for each type of hot spot.

SERS spectra of 1-NAT could be obtained with 633, 785, and 830 nm laser lines. Besides excitation wavelength dependent SERS efficiency of substrates prepared by using larger octahedra (side length 136 ± 6) further confirms the strong field enhancement at 785 nm excitation, where the maximum SERS enhancement is obtained as shown in Supporting Information Figure S7. As the uniformity of SERS substrates is crucial for practical applications, we have investigated spot-to-spot variation by the collection of SERS signals from 15 different random points on the substrates. The results revealed a SERS intensity variation across the substrate only within 5−10%, indicating excellent uniformity (Figure 4b). Additionally, SERS mapping was carried out over an extended area (175 × 100 μm^2) of the three different substrates (Figure 4c−e), observing an excellent uniformity over the whole area. As previously observed, the SERS efficiency increased with the size of Au octahedra (Figure 4c−e). Overall, the SERS substrates prepared by microfluidic-induced self-assembly seems to be very promising for practical applications related to sensing and detection.

CONCLUSIONS

In summary, highly uniform Au octahedra with tight control of size were successfully synthesized in aqueous medium from single-crystalline Au NRs using butenoic acid as reducing agent. The size of the Au octahedra was controlled in a wide range either by simply changing the molar ratio of $HAuCl_4$ to Au seed, single-crystalline NRs or octahedra, (*R*). The success of the synthesis relied on the mild reducing ability of butenoic acid through the oxidation of vinyl group to the corresponding aldehyde or ketone while promoting the thermodynamic growth control. This strategy has been extended to the synthesis of decahedra using pentatwinned Au NRs as seeds. We have also demonstrated the preparation of uniform and large area 3D supercrystal assemblies of Au octahedral NPs in controlled dimensions using a microevaporator device on glass

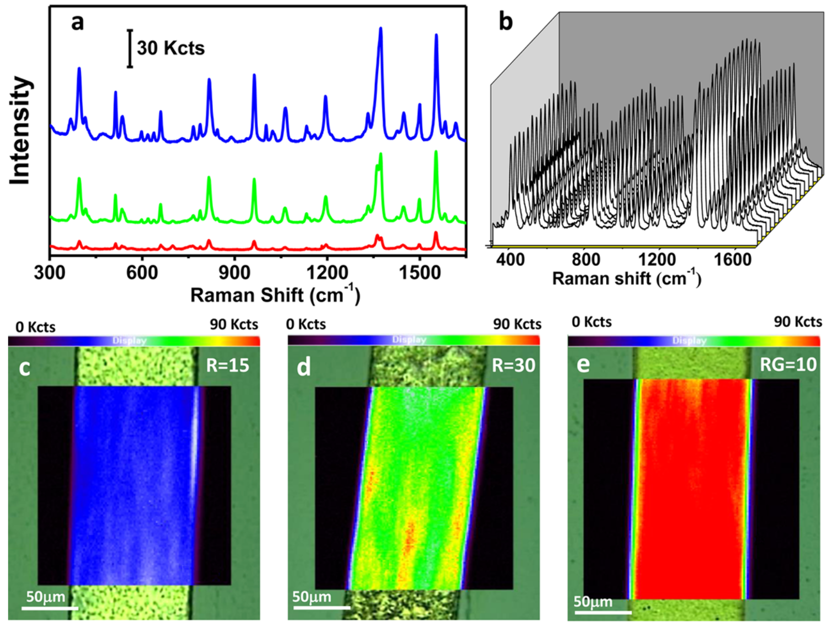

Figure 4. (a) Normalized SERS spectra of 1-NAT obtained with supercrystal fabricated from Au octahedra with average side lengths of 69 ± 5 nm (red), 83 ± 8 nm (green), and 136 ± 6 nm (blue). (b) SERS spectra collected from 15 different points of the substrate fabricated with 136 ± 6 nm Au octahedra. (c−e) Raman confocal image and SERS mapping at 1372 cm^{-1} of the three Au substrates: (c) 69 ± 5 nm, (d) 83 ± 8 nm, and (e) 136 ± 6 nm in side length, using 1-NAT as probe molecule and a 785 nm excitation laser.

substrates. Such substrates exhibit homogeneous SERS activity over large areas, which is a key parameter for quantitative analysis in sensor applications. This work advances the mechanistic understanding of seed-mediated growth for shape-controlled synthesis of metal NPs using well-defined NPs as seeds, and this synthesis approach can be extended to other metal nanocrystals. Furthermore, the microfluidic approach seems to be promising for the fabrication of uniform SERS substrates of any dimensions and it is expected to open doors for the fabrication of SERS substrates for ultrasensitive screening of analytical targets relevant to medical and environmental science.

■ ASSOCIATED CONTENT

Ⓢ Supporting Information

The Supporting Information is available free of charge on the ACS Publications website at DOI: 10.1021/acs.chemmater.5b03620.

> Figures showing the time evolution spectra of the Au(III) to Au(I) reduction. Additional TEM images of the different Au octahedral particles. Electrospray ionization mass spectrum of the reactant and the product. Vis−NIR spectra and TEM images of the particles synthesized in the presence of ascorbic acid and *N*-isopropylacrylamide. Vis−NIR spectra and TEM images of butenoic acid mediated overgrowth of pentatwinned gold nanorods. Normalized SERS spectra of 1-NAT obtained with 633, 785, and 830 cm^{-1} laser lines. (PDF)

■ AUTHOR INFORMATION

Corresponding Authors

*E-mail: pastoriza@uvigo.es.
*E-mail: juste@uvigo.es.

Author Contributions

(S.G.G. and C.F.L) These authors have contributed equally to the work.

Notes

The authors declare no competing financial interest.

■ ACKNOWLEDGMENTS

This work was supported by funding from the Spanish Ministerio de Economía y Competitividad (MAT2013-45168-R) and from the Xunta de Galicia/FEDER (Grant No. GPC2013-006; INBIOMED-FEDER "Unha maneira de facer Europa"). S.G.-G. acknowledges the LabEx AMADEus (ANR-10-LABX-42) in the framework of IdEx Bordeaux (ANR-10-IDEX-03-02).

■ REFERENCES

(1) Lightcap, I. V.; Murphy, S.; Schumer, T.; Kamat, P. V. Electron Hopping through Single-to-Few-Layer Graphene Oxide Films. Side-Selective Photocatalytic Deposition of Metal Nanoparticles. *J. Phys. Chem. Lett.* **2012**, *3*, 1453−1458.

(2) Kamat, P. V. Photophysical, Photochemical and Photocatalytic Aspects of Metal Nanoparticles. *J. Phys. Chem. B* **2002**, *106*, 7729−7744.

(3) Polavarapu, L.; Perez-Juste, J.; Xu, Q.-H.; Liz-Marzan, L. M. Optical Sensing of Biological, Chemical and Ionic Species through Aggregation of Plasmonic Nanoparticles. *J. Mater. Chem. C* **2014**, *2*, 7460−7476.

(4) Mahmoud, M. A.; Garlyyev, B.; El-Sayed, M. A. Controlling the Catalytic Efficiency on the Surface of Hollow Gold Nanoparticles by Introducing an Inner Thin Layer of Platinum or Palladium. *J. Phys. Chem. Lett.* **2014**, *5*, 4088−4094.

(5) DeSantis, C. J.; Weiner, R. G.; Radmilovic, A.; Bower, M. M.; Skrabalak, S. E. Seeding Bimetallic Nanostructures as a New Class of Plasmonic Colloids. *J. Phys. Chem. Lett.* **2013**, *4*, 3072−3082.

(6) Aioub, M.; Kang, B.; Mackey, M. A.; El-Sayed, M. A. Biological Targeting of Plasmonic Nanoparticles Improves Cellular Imaging Via the Enhanced Scattering in the Aggregates Formed. *J. Phys. Chem. Lett.* **2014**, *5*, 2555−2561.

(7) Jiang, R. B.; Li, B. X.; Fang, C. H.; Wang, J. F. Metal/Semiconductor Hybrid Nanostructures for Plasmon-Enhanced Applications. *Adv. Mater.* **2014**, *26*, 5274−5309.

(8) Zhuo, X. L.; Zhu, X. Z.; Li, Q.; Yang, Z.; Wang, J. F. Gold Nanobipyramid-Directed Growth of Length-Variable Silver Nanorods with Multipolar Plasmon Resonances. *ACS Nano* **2015**, *9*, 7523−7535.

(9) Polavarapu, L.; Mourdikoudis, S.; Pastoriza-Santos, I.; Pérez-Juste, J. Nanocrystal Engineering of Noble Metals and Metal Chalcogenides: Controlling the Morphology, Composition and Crystallinity. *CrystEngComm* **2015**, *17*, 3727−3762.

(10) Huang, M. H.; Chiu, C. Y. Achieving Polyhedral Nanocrystal Growth with Systematic Shape Control. *J. Mater. Chem. A* **2013**, *1*, 8081−8092.

(11) Xia, Y.; Xiong, Y.; Lim, B.; Skrabalak, S. E. Shape-Controlled Synthesis of Metal Nanocrystals: Simple Chemistry Meets Complex Physics? *Angew. Chem., Int. Ed.* **2009**, *48*, 60−103.

(12) Murphy, C. J.; Sau, T. K.; Gole, A. M.; Orendorff, C. J.; Gao, J.; Gou, L.; Hunyadi, S. E.; Li, T. Anisotropic Metal Nanoparticles: Synthesis, Assembly, and Optical Applications. *J. Phys. Chem. B* **2005**, *109*, 13857−13870.

(13) Niu, W.; Zhang, L.; Xu, G. Seed-Mediated Growth of Noble Metal Nanocrystals: Crystal Growth and Shape Control. *Nanoscale* **2013**, *5*, 3172−3181.

(14) Gómez-Graña, S.; Goris, B.; Altantzis, T.; Fernández-López, C.; Carbó-Argibay, E.; Guerrero-Martínez, A.; Almora-Barrios, N.; López, N.; Pastoriza-Santos, I.; Pérez-Juste, J.; Bals, S.; Van Tendeloo, G.; Liz-Marzán, L. M. Au@Ag Nanoparticles: Halides Stabilize {100} Facets. *J. Phys. Chem. Lett.* **2013**, *4*, 2209−2216.

(15) Walsh, M. J.; Barrow, S. J.; Tong, W.; Funston, A. M.; Etheridge, J. Symmetry Breaking and Silver in Gold Nanorod Growth. *ACS Nano* **2015**, *9*, 715.

(16) Xia, X.; Xia, Y. Symmetry Breaking During Seeded Growth of Nanocrystals. *Nano Lett.* **2012**, *12*, 6038−6042.

(17) Carbó-Argibay, E.; Rodríguez-González, B.; Pacifico, J.; Pastoriza-Santos, I.; Pérez-Juste, J.; Liz-Marzán, L. M. Chemical Sharpening of Gold Nanorods: The Rod-to-Octahedron Transition. *Angew. Chem., Int. Ed.* **2007**, *46*, 8983−8987.

(18) Wang, Y.; Wan, D.; Xie, S.; Xia, X.; Huang, C. Z.; Xia, Y. Synthesis of Silver Octahedra with Controlled Sizes and Optical Properties Via Seed-Mediated Growth. *ACS Nano* **2013**, *7*, 4586−4594.

(19) Carbó-Argibay, E.; Rodríguez-González, B.; Pastoriza-Santos, I.; Pérez-Juste, J.; Liz-Marzán, L. M. Growth of Pentatwinned Gold Nanorods into Truncated Decahedra. *Nanoscale* **2010**, *2*, 2377−2383.

(20) Liu, W.; Zhang, H.; Wen, T.; Yan, J.; Hou, S.; Shi, X.; Hu, Z.; Ji, Y.; Wu, X. Activation of Oxygen-Mediating Pathway Using Copper Ions: Fine-Tuning of Growth Kinetics in Gold Nanorod Overgrowth. *Langmuir* **2014**, *30*, 12376−12383.

(21) Schlucker, S. Surface-Enhanced Raman Spectroscopy: Concepts and Chemical Applications. *Angew. Chem., Int. Ed.* **2014**, *53*, 4756−4795.

(22) Alvarez-Puebla, R. A.; Liz-Marzán, L. M. Traps and Cages for Universal Sers Detection. *Chem. Soc. Rev.* **2012**, *41*, 43−51.

(23) Alvarez-Puebla, R.; Liz-Marzán, L. M.; de Abajo, F. J. G. Light Concentration at the Nanometer Scale. *J. Phys. Chem. Lett.* **2010**, *1*, 2428−2434.

(24) Solís, D. M.; Taboada, J. M.; Obelleiro, F.; Liz-Marzán, L. M.; de Abajo, F. J. G. Toward Ultimate Nanoplasmonics Modeling. *ACS Nano* **2014**, *8*, 7559−7570.

(25) Chiu, C. Y.; Chen, C. K.; Chang, C. W.; Jeng, U. S.; Tan, C. S.; Yang, C. W.; Chen, L. J.; Yen, T. J.; Huang, M. H. Surfactant-Directed Fabrication of Supercrystals from the Assembly of Polyhedral Au-Pd Core-Shell Nanocrystals and Their Electrical and Optical Properties. *J. Am. Chem. Soc.* **2015**, *137*, 2265−2275.

(26) Alvarez-Puebla, R. A.; Agarwal, A.; Manna, P.; Khanal, B. P.; Aldeanueva-Potel, P.; Carbó-Argibay, E.; Pazos-Pérez, N.; Vigderman, L.; Zubarev, E. R.; Kotov, N. A.; Liz-Marzán, L. M. Gold Nanorods 3d-Supercrystals as Surface Enhanced Raman Scattering Spectroscopy Substrates for the Rapid Detection of Scrambled Prions. *Proc. Natl. Acad. Sci. U. S. A.* **2011**, *108*, 8157−8161.

(27) Gómez-Graña, S.; Pérez-Juste, J.; Alvarez-Puebla, R. A.; Guerrero-Martínez, A.; Liz-Marzán, L. M. Self-Assembly of Au@Ag Nanorods Mediated by Gemini Surfactants for Highly Efficient Sers-Active Supercrystals. *Adv. Opt. Mater.* **2013**, *1*, 477−481.

(28) Huang, M. H.; Thoka, S. Formation of Supercrystals through Self-Assembly of Polyhedral Nanocrystals. *Nano Today* **2015**, *10*, 81−92.

(29) Angly, J.; Iazzolino, A.; Salmon, J.-B.; Leng, J.; Chandran, S. P.; Ponsinet, V.; Désert, A.; Le Beulze, A.; Mornet, S.; Tréguer-Delapierre, M.; Correa-Duarte, M. A. Microfluidic-Induced Growth and Shape-up of Three-Dimensional Extended Arrays of Densely Packed Nanoparticles. *ACS Nano* **2013**, *7*, 6465−6477.

(30) Pérez-Juste, J.; Pastoriza-Santos, I.; Liz-Marzán, L. M. Multifunctionality in Metal@Microgel Colloidal Nanocomposites. *J. Mater. Chem. A* **2013**, *1*, 20−26.

(31) Nikoobakht, B.; El-Sayed, M. A. Preparation and Growth Mechanism of Gold Nanorods (Nrs) Using Seed-Mediated Growth Method. *Chem. Mater.* **2003**, *15*, 1957−1962.

(32) Fernández-López, C.; Polavarapu, L.; Solís, D. M.; Taboada, J. M.; Obelleiro, F.; Contreras-Cáceres, R.; Pastoriza-Santos, I.; Pérez-Juste, J. Gold Nanorod−Pnipam Hybrids with Reversible Plasmon Coupling: Synthesis, Modeling, and Sers Properties. *ACS Appl. Mater. Interfaces* **2015**, *7*, 12530−12538.

(33) Merlin, A.; Salmon, J.-B.; Leng, J. Microfluidic-Assisted Growth of Colloidal Crystals. *Soft Matter* **2012**, *8*, 3526−3537.

(34) Rodríguez-Fernández, J.; Pérez-Juste, J.; Mulvaney, P.; Liz-Marzán, L. M. Spatially-Directed Oxidation of Gold Nanoparticles by Au(Iii)-Ctab Complexes. *J. Phys. Chem. B* **2005**, *109*, 14257−14261.

(35) Yavuz, M. S.; Li, W.; Xia, Y. Facile Synthesis of Gold Icosahedra in an Aqueous Solution by Reacting Haucl4 with N-Vinyl Pyrrolidone. *Chem. - Eur. J.* **2009**, *15*, 13181−13187.

(36) Wickens, Z. K.; Skakuj, K.; Morandi, B.; Grubbs, R. H. Catalyst-Controlled Wacker-Type Oxidation: Facile Access to Functionalized Aldehydes. *J. Am. Chem. Soc.* **2014**, *136*, 890−893.

(37) Carbó-Argibay, E.; Rodríguez-González, B.; Gómez-Grana, S.; Guerrero-Martinez, A.; Pastoriza-Santos, I.; Pérez-Juste, J.; Liz-Marzán, L. M. The Crystalline Structure of Gold Nanorods Revisited: Evidence for Higher-Index Lateral Facets. *Angew. Chem., Int. Ed.* **2010**, *49*, 9397−9400.

(38) Leng, J.; Lonetti, B.; Tabeling, P.; Joanicot, M.; Ajdari, A. Microevaporators for Kinetic Exploration of Phase Diagrams. *Phys. Rev. Lett.* **2006**, *96*, 084503.

(39) Hamon, C.; Novikov, S.; Scarabelli, L.; Basabe-Desmonts, L.; Liz-Marzán, L. M. Hierarchical Self-Assembly of Gold Nanoparticles into Patterned Plasmonic Nanostructures. *ACS Nano* **2014**, *8*, 10694−10703.

(40) Polavarapu, L.; Liz-Marzán, L. M. Towards Low-Cost Flexible Substrates for Nanoplasmonic Sensing. *Phys. Chem. Chem. Phys.* **2013**, *15*, 5288−5300.

(41) Polavarapu, L.; Porta, A. L.; Novikov, S. M.; Coronado-Puchau, M.; Liz-Marzán, L. M. Pen-on-Paper Approach toward the Design of Universal Surface Enhanced Raman Scattering Substrates. *Small* **2014**, *10*, 3065−3071.